

**REPORT DOCUMENTATION PAGE**

Form Approved OMB No. 0704-0188

Public reporting burden for this collection of information is estimated to average 1 hour per response, including the time for reviewing instructions, searching existing data sources, gathering and maintaining the data needed, and completing and reviewing the collection of information. Send comments regarding this burden estimate or any other aspect of this collection of information, including suggestions for reducing the burden, to Department of Defense, Washington Headquarters Services, Directorate for Information Operations and Reports (0704-0188), 1215 Jefferson Davis Highway, Suite 1204, Arlington, VA 22202-4302. Respondents should be aware that notwithstanding any other provision of law, no person shall be subject to any penalty for failing to comply with a collection of information if it does not display a currently valid OMB control number.  
**PLEASE DO NOT RETURN YOUR FORM TO THE ABOVE ADDRESS.**

<b>1. REPORT DATE (DD-MM-YYYY)</b> 08-12-2003	<b>2. REPORT TYPE</b> Final Report	<b>3. DATES COVERED (From - To)</b> 16 September 2002 - 13-Feb-04
--	---------------------------------------	--

<b>4. TITLE AND SUBTITLE</b>  Gan/Algan Strain-Balanced Heterostructures For Near-IR Quantum Well Photodetectors	<b>5a. CONTRACT NUMBER</b> FA8655-02-M4006
	<b>5b. GRANT NUMBER</b>
	<b>5c. PROGRAM ELEMENT NUMBER</b>

<b>6. AUTHOR(S)</b>  Dr. Paul Harrison	<b>5d. PROJECT NUMBER</b>
	<b>5d. TASK NUMBER</b>
	<b>5e. WORK UNIT NUMBER</b>

<b>7. PERFORMING ORGANIZATION NAME(S) AND ADDRESS(ES)</b> University of Leeds School of Electronic and Electrical Engineers Leeds LS2 9JT United Kingdom	<b>8. PERFORMING ORGANIZATION REPORT NUMBER</b>  N/A
--	--

<b>9. SPONSORING/MONITORING AGENCY NAME(S) AND ADDRESS(ES)</b>  EOARD PSC 802 BOX 14 FPO 09499-0014	<b>10. SPONSOR/MONITOR'S ACRONYM(S)</b>
	<b>11. SPONSOR/MONITOR'S REPORT NUMBER(S)</b> SPC 02-4006

**12. DISTRIBUTION/AVAILABILITY STATEMENT**  
Approved for public release; distribution is unlimited.

**13. SUPPLEMENTARY NOTES**

**14. ABSTRACT**  
  
This report results from a contract tasking University of Leeds as follows: The contractor will design, fabricate, and analyze Quantum Well Infrared Photodetectors (QWIP) that detect in the 2-6 micron region. The QWIPs performance will be compared to standard MerCad Telluride (HgCdTe) photodetector devices working in the same wavelength region.

**15. SUBJECT TERMS**  
EOARD, Sensor Technology, infrared technology, Gallium Nitride, Quantum Well Devices

<b>16. SECURITY CLASSIFICATION OF:</b>			<b>17. LIMITATION OF ABSTRACT</b> UL	<b>18. NUMBER OF PAGES</b>	<b>19a. NAME OF RESPONSIBLE PERSON</b> CARL A. KUTSCHE, Lt Col, USAF
<b>a. REPORT</b> UNCLAS	<b>b. ABSTRACT</b> UNCLAS	<b>c. THIS PAGE</b> UNCLAS			<b>19b. TELEPHONE NUMBER (Include area code)</b> +44 (0)20 7514 4505

GaN/AlGaN strain-balanced heterostructures for near-IR  
quantum well photodetectors:  
Final report  
Contract: FA8655-02-M4006

P. Harrison,  
IMP, School of Electronic and Electrical Engineering,  
University of Leeds, LS2 9JT, U.K.

December 3, 2003

**Abstract**

This is the final report for a 1-year project funded by the European Office of Research and Development (EOARD). In this work GaN/AlGaN strain-balanced heterostructures have been designed for near-infrared absorption through *intersubband* transitions. By making use of existing collaborations with workers at the University of Sheffield and UMIST the semiconductor samples have been grown, characterised and fabricated into devices. The experimental results have been used to validate the design procedure and the prototype devices resulting from these collaborations are the first quantum well infrared photodetectors based in the GaN material system to be reported.

1. In accordance with Defense Federal Acquisition Regulation 252.227-7036, Declaration of Technical Data Conformity (Jan 1997) :

"The Contractor, University of Leeds, hereby declares that, to the best of its knowledge and belief, the technical data delivered herewith under Contract No. F61775-01-WE088 is complete, accurate, and complies with all requirements of the contract."

DATE: 03/12/03 (3rd December 2003)

Name and Title of Authorized Official: Prof. P. Harrison

2. In accordance with the requirements in Federal Acquisition Regulation 52.227-13, Patent Rights-Acquisition by the U.S. Government (Jun 1989) : "Disclosures of all subject inventions as defined in FAR 52.227-13 have been reported in accordance with this clause."

DATE: 03/12/03 (3rd December 2003)

Name and Title of Authorized Official: Prof. P. Harrison

## 1 Summary of scientific achievements

1. Developed a model for calculating the conduction band potential profile of a GaN/Ga<sub>1-x</sub>Al<sub>x</sub>N heterostructure including the spontaneous polarisation and piezoelectric fields[1]
2. Applied the model to the design of quantum wells for use in intersubband devices at near-infrared wavelengths [1]
3. Designed quantum well systems for near-infrared absorption at 2, 3, 4 and 5  $\mu\text{m}$  for use in model validation experiments[2]
4. Quantum well samples were grown by chemical vapour deposition by our collaborator Peter Parbrook at the University of Sheffield and characterised with Raman spectroscopy and photoluminescence by our collaborator Matthew Halsall at UMIST[2]
5. Quantum well infrared photodetectors (QWIPs) were fabricated at UMIST and photocurrent measurements were performed
6. A model of the dark (noise) current based on full self-consistent solution of the subband rate equations was developed for QWIPs. This was validated by comparison with experiment[3]

## 2 Scientific Conclusions

A model for the electron energy levels in strain-balanced GaN/AlGa<sub>x</sub>N heterostructures has been developed and validated by comparison with experiment. The model has been used to design quantum well structures for photoabsorption in the near-infrared spectral range. With the aid of collaborators these semiconductor heterostructures have been grown and fabricated into the first GaN QWIPs. In addition, the first fully dynamical model of the dark and light currents in QWIPs has been developed and applied to the calculation of the noise current and responsivity. The results of these calculations have also been validated by experiment.

## 3 List of publications (attached)

1. V. D. Jovanović, Z. Ikonić, D. Indjin, P. Harrison, V. Milanović, and R. A. Soref, *Designing strain-balanced GaN/AlGa<sub>x</sub>N quantum well structures: Application to intersubband devices at 1.3 and 1.55  $\mu\text{m}$* , J. Appl. Phys., 93:3194 (2003)
2. M. P. Halsall, B. Sherliker, P. Harrison, V. D. Jovanović, D. Indjin, Z. Ikonić, T. Wang, M. A. Whitehead, and P. J. Parbrook, *Electronic Raman scattering from intersubband transitions in GaN/AlGa<sub>x</sub>N quantum wells*, phys. stat. sol. (c), 0:2662–2665 (2003)
3. V. Jovanović, D. Indjin, Z. Ikonić, P. Harrison and R. A. Soref, *Simulation and design of GaN-based near infrared quantum well infrared photodetectors (QWIPs)*, in draft form

## 4 List of conference presentations and seminars

1. **Condensed Matter and Materials Physics**, Belfast, April 2003, '*Design issues for GaN intersubband devices*', presented by V. Jovanović
2. **7th International Conference on Intersubband Transitions in Quantum Wells**, Switzerland, September 2003, ' *$\lambda \sim 3.5\mu\text{m}$  intersubband transitions and electronic Raman scattering study in strain balanced GaN/AlGaN quantum wells*', presented by V. Jovanovic
3. **U.K. Nitrides Consortium Meeting**, Cardiff, June 2003, '*Recent progress in GaN/AlGaN intersubband devices design*'

## 5 Suggestions for future projects

This project has been a feasibility study to see if GaN-based QWIPs with sufficiently large conduction band offset could be designed for near-infrared absorption. The scientific output of the project has demonstrated that this is the case and this has been further substantiated with the growth and characterisation of several samples. This work is now at a crossroads and as this report is written no funds have been secured with which to continue this unique and leading work.

The opportunity is therefore taken in this final report to suggest potential projects and the required level of funding in order to meet certain targets:

1. **Optimised uncooled near-infrared single-pixel detectors operating across the 1–5  $\mu\text{m}$  wavelengths** In this project the first GaN-based QWIPs have been designed, fabricated and characterised. The short duration of the project (1 year) and the limited budget have only allowed for one iteration in the design and fabrication cycle and further improvements in the performance of the devices would require further time and funding. A three year programme with 3 PhD students would be an effective way to continue in this line of research and it is likely that the objective of uncooled detection of near-infrared radiation could be achieved with a single pixel device.  
**Funding required: Around \$100k/year for 3 years**
2. **Focal plane arrays (FPAs) for near-infrared imaging and spectroscopy** This more ambitious aim would be attempted as a follow on from the above. This would require the optimisation of the single pixel detectors and then the development of the fabrication technologies to achieve large scale (10,000-100,000) arrays of pixels for connection to commercially available readout circuits and cameras. This has been achieved in a selection of other materials including GaAs- and HgCdTe-based devices. The resources required for this are likely to be 2 Postdoctoral level researchers for 3 years. **Funding required: Around \$150k/year for 3 years**

# Designing strain-balanced GaN/AlGaIn quantum well structures: Application to intersubband devices at 1.3 and 1.55 $\mu\text{m}$ wavelengths

V. D. Jovanović,<sup>a)</sup> Z. Ikonić, D. Indjin, and P. Harrison  
*School of Electronic and Electrical Engineering, University of Leeds, Leeds LS2 9JT, United Kingdom*

V. Milanović  
*School of Electrical Engineering, Bulevar Kralja Aleksandra 73, 11120 Belgrade, Yugoslavia*

R. A. Soref  
*Sensor Directorate, Air Force Research Laboratory, AFRL/SNHC, Hanscom Air Force Base, Massachusetts 01731*

(Received 3 December 2002; accepted 8 January 2003)

A criterion for strain balancing of wurtzite group-III nitride-based multilayer heterostructures is presented. Single and double strain-balanced GaN/AlGaIn quantum well structures are considered with regard to their potential application in optoelectronic devices working at communication wavelengths. The results for realizable, strain-balanced structures are presented in the form of design diagrams that give both the intersubband transition energies and the dipole matrix elements in terms of the structural parameters. The optimal parameters for structures operating at  $\lambda \sim 1.3$  and  $1.55 \mu\text{m}$  were extracted and a basic proposal is given for a three level intersubband laser system emitting at  $1.55 \mu\text{m}$  and depopulating via resonant longitudinal optical (LO) phonons ( $\hbar\omega_{\text{LO}} \approx 90 \text{ meV}$ ). © 2003 American Institute of Physics. [DOI: 10.1063/1.1556177]

## I. INTRODUCTION

In recent years intersubband transitions (ISBTs) in AlGaIn-based heterostructures have emerged as a promising route for access to the near-infrared spectral range, while also showing ultrafast carrier dynamics. A few groups have reported intersubband absorption for wavelengths around 1.3 and  $1.55 \mu\text{m}$ ,<sup>1-7</sup> that are important for optoelectronic telecommunications, as well as ultrashort relaxation times  $\tau_{\text{rel}} \sim \text{fs}$  in quantum well structures and superlattices.<sup>8-10</sup> These experimental successes suggest possible application in quantum well infrared photodetectors (QWIPs), optical switches or even intersubband lasers. Improvements in the molecular beam epitaxy growth technique that allow control of layer widths of the order of a few monolayers make feasible the design and growth of complex structures. However, growth of uniform, dislocation-free multilayer, optically thick stacks is still a considerable challenge.<sup>11,12</sup> To achieve pseudomorphic growth, there is the requirement of strain balance upon the whole structure. Although multilayer structures generally show much better stability against relaxation than do homogeneous strained layers, one should still aim at achieving full strain balance when designing such a structure in order to have reliable, reproducible growth.

Several approaches to the design of strain-balanced structures have been considered,<sup>13</sup> but they were usually restricted to two-layer structures (e.g., single quantum wells) based upon semiconductor materials with cubic symmetry. In this article we extend the “zero-strain” approach<sup>13</sup> to multilayer structures based upon wurtzite (e.g., GaN/AlIn) semiconductors grown in the conventional [0001] direction,

and then we present design diagrams oriented their possible application in optoelectronics.

## II. THEORETICAL CONSIDERATIONS

The zero-strain condition<sup>13</sup> is the only theoretical approach that accounts for different elastic constants of layers, in contrast to the more common average lattice or thickness weighted methods.<sup>14</sup> It is based on minimizing the average elastic energy for the whole multilayer structure, i.e.,

$$\bar{f} = \frac{\sum_{k=1}^n f_k l_k}{\sum_{k=1}^n l_k}, \quad (1)$$

where  $l_k$  is the width and  $f_k$  strain energy density of the  $k$ th layer.

Within the framework of classical elastic theory<sup>15</sup> the elastic energy density of the  $k$ th layer is

$$f_k = \sum_{i=1}^6 \sum_{j=1}^6 \frac{1}{2} c_{ij}^{(k)} \epsilon_i^{(k)} \epsilon_j^{(k)}, \quad (2)$$

where  $c_{ij}^{(k)}$  is the elastic tensor element and  $\epsilon_{i,j}^{(k)}$  the strain tensor element for a hexagonal crystallographic system in matrix notation<sup>15</sup> of the  $k$ th layer.

Since we consider a wurtzite based multilayer system grown along the [0001] axis, the corresponding stress tensor element ( $\sigma_3$ ) should equal zero. By using formulas given in Refs. 15 and 16 the biaxial strain tensor has only diagonal elements and is given by

$$\epsilon = \begin{bmatrix} \epsilon_1 & \epsilon_6 & \epsilon_5 \\ \epsilon_6 & \epsilon_1 & \epsilon_4 \\ \epsilon_5 & \epsilon_4 & \epsilon_3 \end{bmatrix} = \begin{bmatrix} \epsilon_1 & 0 & 0 \\ 0 & \epsilon_1 & 0 \\ 0 & 0 & -2 \frac{c_{13}}{c_{33}} \epsilon_1 \end{bmatrix}, \quad (3)$$

<sup>a)</sup>Electronic mail: eenvj@leeds.ac.uk

where  $\epsilon_1 = (a - a_0)/a_0$  is the in-plane strain,  $a$  is the buffer in-plane lattice constant (along the wurtzite  $a$  axis) and  $a_0$  is the lattice constant of a layer in strain-free conditions. From Eqs. (2) and (3) it follows that the strain energy density in a layer is

$$f_k = A_k \cdot [\epsilon_1^{(k)}]^2, \tag{4}$$

where  $A = c_{11} + c_{12} - 2c_{13}^2/c_{33}$ . Equation (1) may then be written as

$$\bar{f} = \frac{\sum_{k=1}^n A_k [\epsilon_1^{(k)}]^2 l_k}{\sum_{k=1}^n l_k}. \tag{5}$$

The pseudomorphic condition relates the strain in adjacent layers ( $\epsilon_1^{(k)}$  and  $\epsilon_1^{(k-1)}$ ) and is given as

$$\epsilon_1^{(k)} = \frac{a_{k-1}}{a_k} \epsilon_1^{(k-1)} + \frac{a_{k-1} - a_k}{a_k}, \tag{6}$$

and the average in-plane stress that follows is

$$\begin{aligned} \bar{\sigma} &= \frac{\partial \bar{f}}{\partial \epsilon_1^{(1)}} = \frac{2}{l_1 + l_2 + l_3 + \dots}, \\ &\times \left\{ A_1 \epsilon_1^{(1)} l_1 + A_2 \epsilon_1^{(2)} l_2 \frac{\partial \epsilon_1^{(2)}}{\partial \epsilon_1^{(1)}} + A_3 \epsilon_1^{(3)} l_3 \frac{\partial \epsilon_1^{(3)}}{\partial \epsilon_1^{(1)}} + \dots \right\}. \end{aligned} \tag{7}$$

The zero-stress (or strain-balance) condition means that the in-plane stress is zero, and using  $\partial \epsilon_1^{(k)}/\partial \epsilon_1^{(1)} = a_1/a_k$  ( $k = 2, 3, \dots$ ) Eq. (7) then gives

$$A_1 \epsilon_1^{(1)} l_1 + A_2 \epsilon_1^{(2)} l_2 \frac{a_1}{a_2} + A_3 \epsilon_1^{(3)} l_3 \frac{a_1}{a_3} + \dots = 0, \tag{8}$$

which delivers the buffer lattice constant necessary for the strain-balanced multilayer structure as

$$a_0 = \frac{\sum_{k=1}^n A_k l_k / a_k}{\sum_{k=1}^n A_k l_k / a_k^2}, \tag{9}$$

and, therefore, in case of GaN/AlGaIn structures, the Al content in the buffer follows straightforwardly.

If a multilayer structure has periodicity, the above expression should be understood to apply to  $n$  layers that constitute a single period, and the whole structure will then clearly be strain balanced.

The strain level in individual layers directly influences the conduction band profile, due to the large strain-dependent, piezoelectric polarization induced electric field.<sup>17</sup> This means that strain-balanced device design and optimization are more complicated than would be the case with no polarization. This is because any single structural parameter cannot be varied independently (in order to change the sub-band structure), so the strain-balance condition has to be met as well. In the remaining part of this article, we present suitable design diagrams for strain-balanced single and double GaN/AlGaIn QW structures; see Fig. 1. Single QW structures were explored with respect to the ISBT energies and dipole matrix elements corresponding to the  $1 \rightarrow 2$  transition with a view towards their possible application in devices like QWIPs or saturable switches. Double QWs were explored

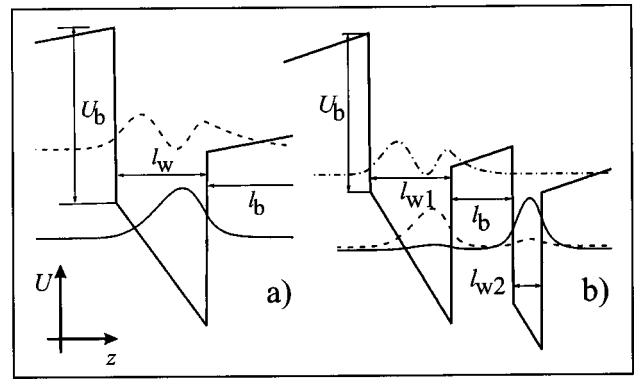


FIG. 1. Conduction band profile and wave function moduli of single and coupled double GaN/AlGaIn QWs, and the notation of structural parameters.

with respect to transition energies between  $|1\rangle$  and  $|2\rangle$ , and  $|2\rangle$  and  $|3\rangle$ , with a view towards their potential application in three-level intersubband lasers.<sup>18</sup>

In the calculations we have employed the effective mass model and solved the envelope function Schrödinger equation with bulk nonparabolicity included via the energy dependent effective mass (two band Kane model).<sup>19</sup> Nonlinear piezoelectric and spontaneous polarizations were also included<sup>20</sup> and the fields induced were calculated from the simple expression<sup>21</sup> (all constraints of that approach are satisfied here<sup>22</sup>)

$$F_j = \frac{\sum_k (P_k - P_j) l_k / \epsilon_k}{\epsilon_j \sum_k l_k / \epsilon_k}, \tag{10}$$

where  $P_i = P_{sp}^i + P_{pz}^i$  is the total polarization given as a sum of piezoelectric and spontaneous (pyroelectric) polarization within a layer of width  $l_i$ . In calculating the alloy band gap we have included the effect of bowing.<sup>23</sup>

The Schrödinger equation used within this model is

$$-\frac{\hbar^2}{2} \frac{\partial}{\partial z} \left( \frac{1}{m(z, E)} \frac{d\Psi}{dz} \right) + U(z)\Psi = E\Psi, \tag{11}$$

where the position- and energy-dependent effective mass is  $m(z, E) = m(z) \{1 + [E - U(z)]/E_g(z)\}$ , where  $m(z)$ ,  $E_g(z)$  and  $U(z)$  denote, respectively, the parabolic effective mass, band gap and conduction band edge (which includes the band edge discontinuities and the polarization-induced potential). All three vary along coordinate  $z$  because of modulation of the material composition. This equation may be solved by a standard shooting method, starting with a well-behaved wave function on one side and scanning for energies where it is well behaved on the other side. However, this method loses stability for wider structures, typically with those five wells or so. We have therefore employed a finite-difference method, in which Eq. (11) is written in discretized form, in  $N_z$  points along the  $z$  axis like, e.g., in Ref. 24, and reduces to a matrix eigenvalue problem, where the Hamiltonian matrix is tridiagonal. However, the energy  $E$  appears not only in the main diagonal, but in all the terms (via the effective mass), which leads to a nonlinear eigenvalue problem,

$$[H(E)]\psi = E\psi, \tag{12}$$

which cannot be solved by conventional diagonalization routines that handle linear eigenvalue problems  $[H]\psi = E\psi$  (which would be the case if the Hamiltonian, i.e., the effective mass in it, is not energy dependent). In the field of electronic structure calculations nonlinear eigenvalue problems also appear, e.g., in augmented plane wave methods, but the matrix there is not tridiagonal, and the computational demands are considerably larger than for linear eigenproblems, so sophisticated methods have been devised to speed up the process.<sup>25</sup> Here, however, we take advantage of the tridiagonal form of the finite-difference representation Eq. (11) for fast solving of Eq. (12). We first scan for energies  $E_i$  where

$$\det([H(E_i)] - E_i[I]) = 0 \quad (13)$$

is satisfied [the  $E_i$  are obviously the eigenvalues of Eq. (12) and  $[I]$  is the  $N_z \times N_z$  unity matrix]. Calculation of the determinant of the tridiagonal matrix<sup>26</sup> is fast and scales linearly with its size  $N_z$  (just as does the shooting method), hence it is easy to achieve high precision. In this particular problem it suffices to find just the sign, not the full value of the determinant, and supply it to the bisection routine, a feature which almost cuts into half the computational time. Normally, one is interested in only a few lowest, rather than all,  $N_z$  eigenvalues of Eq. (12).

To find the eigenvectors, i.e., the wave functions, Eq. (12) can be written, for any particular  $E_i$  in the form of a fictitious linear eigenproblem,

$$([H(E_i)] - E_i[I])\psi_i = \lambda\psi_i. \quad (14)$$

One of the  $N_z$  eigenvalues  $\lambda$  will be (almost, because of roundoff errors) equal to zero, and the eigenvector corresponding to it is actually the eigenvector of Eq. (12) corresponding to eigenenergy  $E_i$  [other eigenvalues and eigenvectors of Eq. (14) are physically meaningless]. For this task we use standard diagonalization routines (EISPACK) that allow evaluation of a single, selected eigenvector—that with the already known, zero eigenvalue. Alternatively, upon finding eigenvalues  $E_i$ , one may also calculate eigenvectors by solving the tridiagonal system of linear equations corresponding to Eq. (12) using appropriate fast routines,<sup>26</sup> but this approach was found to offer somewhat less stability.

The method was found to be about as equally fast and accurate as the shooting method (in cases where both work well), while retaining full stability where the shooting method fails.

The calculated results were used to make contour plots, from which the sets of structural parameters that deliver the transition energy or matrix element of interest may be easily read, thus allowing some optimal choice to be made.

### III. NUMERICAL RESULTS AND DISCUSSION

Figure 2 shows contour plots of both the ISBT energies and dipole matrix elements squared, corresponding to the  $1 \rightarrow 2$  transition in a single QW structure as functions of the relevant structural parameters [for the notation see Fig. 1(a)], i.e., the well width ( $l_w$ ) and the Al content in the barrier layer ( $x_b \approx U_b / \Delta E_c$ , where  $\Delta E_c$  is the conduction band off-

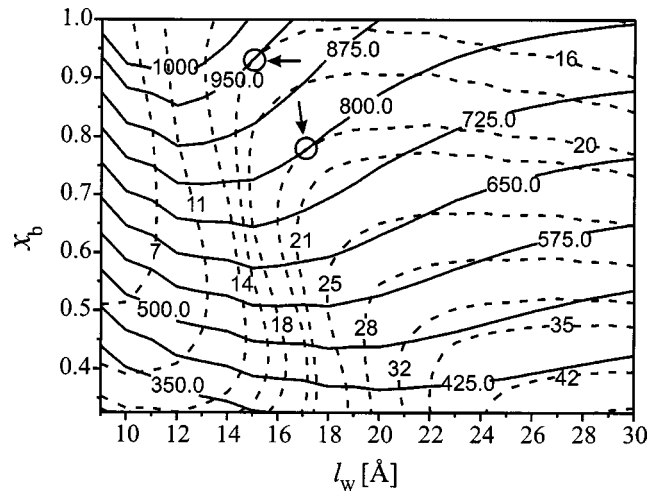


FIG. 2. Contour plot of the transition energies (solid line) and dipole matrix element squared (dashed line) between levels  $|1\rangle$  and  $|2\rangle$  in single AlGaIn/GaN QWs obtained for a range of structural parameters.

set set to 2 eV).<sup>27,28</sup> A fixed value of the barrier width was chosen as  $l_b = 60$  Å since it does not influence the results much.

In order to give specific examples, we consider the cases of 1.3 ( $\sim 950$  meV) and  $1.55\mu\text{m}$  ( $\sim 800$  meV) transitions, which are important in applications. The structural parameters that deliver the  $1.55\mu\text{m}$  intersubband absorption can be read from the solid line labeled 800.0 (in units of meV) in Fig. 2. Any choice along this line gives the same wavelength, but the dipole matrix element  $d_{12}$  varies. There are two sets giving, e.g.,  $d_{12}^2 = 16$  Å<sup>2</sup>; these are at the intersections of the dashed line labeled 16 with the 800.0 solid line. Usually one aims to have the largest possible  $d_{12}$ , and these (optimal) structural parameters occur where a dashed line just touches the 800.0 solid line: in this case it is the dashed line labeled 20, i.e., the maximal value of  $d_{12}^2 = 20$  Å<sup>2</sup> and it is obtained with  $l_w = 18$  Å and  $x_b = 0.8$  (this point is marked by a circle and an arrow in Fig. 2). Similarly, one can see from Fig. 2 that the absorption at  $1.3\mu\text{m}$  can be achieved only in a rather narrow range of parameters:  $l_w \leq 17$  Å and  $x_b > 0.85$ , and the largest possible value of  $d_{12}^2 = 16$  Å<sup>2</sup> is obtained for  $l_w = 17$  Å and  $x_b = 0.94$  (also marked in Fig. 2). Along with the optimal parameters, Fig. 2 shows the range of parameters that can provide any (suboptimal) structure for a given wavelength, and also indicates where the sensitivity to a parameter becomes only marginal. These may be important when the optimal design cannot be fabricated, for whatever reason.

The contour plots shown in Figs. 3 and 4 show ISBT energies corresponding to the  $1 \rightarrow 2$  and  $2 \rightarrow 3$  transitions in double QW structures as a function of their structural parameters [for the notation see Fig. 1(b)], i.e., the first well ( $l_{w1}$ ) and middle barrier width ( $l_b$ ), for two fixed values of the second well width ( $l_{w2} = 6$  and  $8$  Å). In this calculation the outer barriers were chosen to be of AlN, in order to accommodate the three states, and their widths were also set to 60 Å. An interesting case, in view of the possible application of double QW systems as active regions of intersubband lasers, occurs when the energy of the  $1 \rightarrow 2$  transition is close to the longitudinal optical (LO) phonon energy ( $\hbar\omega_{\text{LO}} \approx 90$  meV in

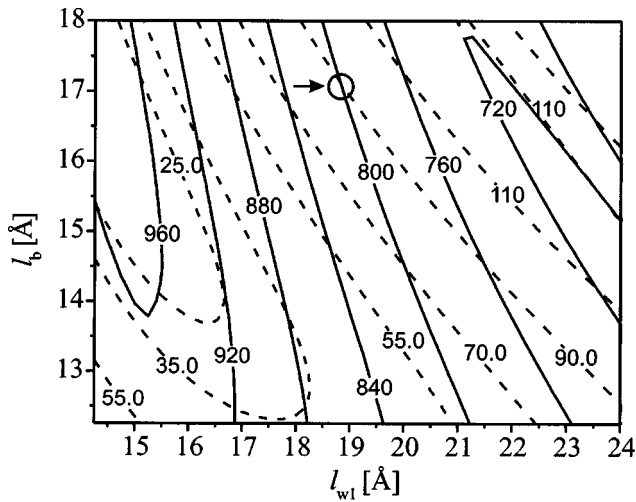


FIG. 3. Contour plot of transition energies between  $|1\rangle$  and  $|2\rangle$  (dashed line) and  $|2\rangle$  and  $|3\rangle$  (solid line) states in double AlN/GaN QWs obtained for a range of structural parameters. The second well width is set to  $l_{w2} = 6 \text{ \AA}$ .

GaN). This provides ultrafast depopulation of the second subband and the possibility of population inversion between levels  $|3\rangle$  and  $|2\rangle$ . An interesting choice is if the spacing between the second and third subband is set to a wavelength of  $1.55 \mu\text{m}$ , which is important in fiber-based communications. For  $l_{w2} = 6 \text{ \AA}$  this situation appears for the first well width of  $l_{w1} = 19 \text{ \AA}$  and the middle barrier width of  $17 \text{ \AA}$ . A wider second well ( $l_{w2} = 8 \text{ \AA}$ ) requires a much wider first well,  $l_{w1} = 29 \text{ \AA}$ , while the middle barrier width is  $l_b = 16 \text{ \AA}$ . That is a direct consequence of the presence of polarization induced fields in the layers and the therefore inherent tilt of the structure.

For any set of parameters from these diagrams, the strain-balance requirement can be straightforwardly determined from Eq. (9).

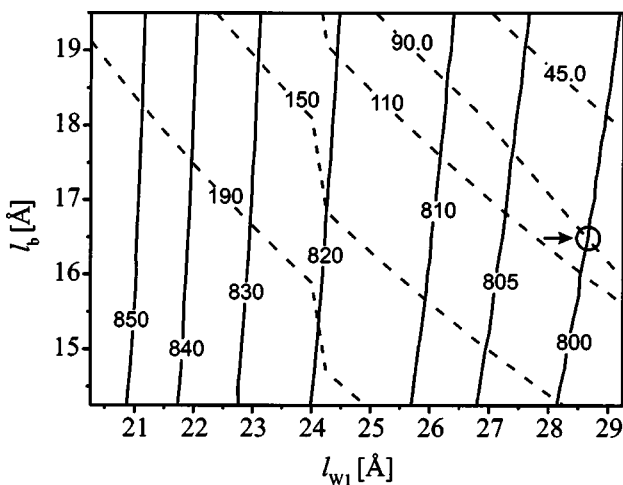


FIG. 4. Same as in Fig. 3, but for  $l_{w2} = 8 \text{ \AA}$ .

#### IV. CONCLUSION

A strain-balance condition for wurtzite GaN-based multilayer structures was been derived and useful, “design-friendly” contour plots for single and double QW structures complying with the strain-balance requirement are given. From these plots optimal parameters were extracted for ISBT absorption-based devices, as well as for a candidate structure for a three level intersubband laser.

#### ACKNOWLEDGMENTS

The authors would like to thank the Royal Society, EOARD and AFOSR for funding. One of the authors (V.D.J.) was supported by an ORS award.

- <sup>1</sup>C. Gmachl, H. M. Ng, S.-N. G. Chu, and A. Y. Cho, *Appl. Phys. Lett.* **77**, 3722 (2000).
- <sup>2</sup>C. Gmachl, H. M. Ng, and A. Y. Cho, *Appl. Phys. Lett.* **77**, 334 (2000).
- <sup>3</sup>C. Gmachl, H. M. Ng, and A. Y. Cho, *Appl. Phys. Lett.* **79**, 1590 (2001).
- <sup>4</sup>C. Gmachl, S. V. Frolov, H. M. Ng, S.-N. G. Chu, and A. Y. Cho, *Electron. Lett.* **37**, 378 (2001).
- <sup>5</sup>N. Iizuka, K. Kaneko, and N. Suzuki, *Appl. Phys. Lett.* **81**, 1803 (2002).
- <sup>6</sup>K. Kishino, A. Kikuchi, H. Kanazawa, and T. Tachibana, *Appl. Phys. Lett.* **81**, 1234 (2002).
- <sup>7</sup>K. Kishino, A. Kikuchi, H. Kanazawa, and T. Tachibana, *Phys. Status Solidi A* **192**, 124 (2002).
- <sup>8</sup>N. Iizuka, K. Kaneko, N. Suzuki, T. Asano, S. Noda, and O. Wada, *Appl. Phys. Lett.* **77**, 648 (2000).
- <sup>9</sup>J. D. Heber, C. Gmachl, H. M. Ng, and A. Y. Cho, *Appl. Phys. Lett.* **81**, 1237 (2002).
- <sup>10</sup>H. M. Ng, C. Gmachl, S. V. Frolov, S. N. G. Chu, and A. Y. Cho, *IEEE Proc.: Optoelectron.* **148**, 215 (2001).
- <sup>11</sup>A. Y. Cho, D. L. Sivco, H. M. Ng, C. Gmachl, A. Tredicucci, A. L. Hutchinson, S. N. G. Chu, and F. Capasso, *J. Cryst. Growth* **227–228**, 1 (2001).
- <sup>12</sup>H. M. Ng, C. Gmachl, S. N. G. Chu, and A. Y. Cho, *J. Cryst. Growth* **220**, 432 (2000).
- <sup>13</sup>N. J. Ekins-Daukes, K. Kawaguchi, and J. Zhang, *Cryst. Growth Design* **2**, 287 (2002).
- <sup>14</sup>N. J. Ekins-Daukes *et al.*, *Sol. Energy Mater. Sol. Cells* **68**, 71 (2001).
- <sup>15</sup>J. F. Nye, *Physical Properties of Crystals: Their Representation by Tensors and Matrices* (Oxford University Press, London, 1985).
- <sup>16</sup>O. Ambacher *et al.*, *J. Phys.: Condens. Matter* **14**, 3399 (2002).
- <sup>17</sup>V. Fiorentini, F. Bernardini, F. Della Sala, A. Di Carlo, and P. Lugli, *Phys. Rev. B* **60**, 8849 (1999).
- <sup>18</sup>H. C. Liu, I. W. Cheung, A. J. Spring Thorpe, C. Dharma-Wardana, Z. R. Wasilewski, D. J. Lockwood, and G. C. Aers, *Appl. Phys. Lett.* **78**, 3580 (2001).
- <sup>19</sup>V. Jovanović, D. Indjin, Z. Ikončić, V. Milanović, and J. Radovanović, *Solid State Commun.* **121**, 619 (2002), and references therein.
- <sup>20</sup>V. Fiorentini, F. Bernardini, and O. Ambacher, *Appl. Phys. Lett.* **80**, 1204 (2002).
- <sup>21</sup>F. Bernardini and V. Fiorentini, *Appl. Surf. Sci.* **166**, 23 (2000).
- <sup>22</sup>F. Bernardini and V. Fiorentini, *Phys. Status Solidi B* **216**, 391 (1999).
- <sup>23</sup>F. Yun, M. A. Reshchikov, L. He, T. King, and H. Morkoç, *J. Appl. Phys.* **92**, 4837 (2002).
- <sup>24</sup>P. Harrison, *Quantum Wells, Wires and Dots: Theoretical and Computational Physics* (Wiley, Chichester, UK, 1999).
- <sup>25</sup>E. Sjösted and L. Nordström, *J. Phys.: Condens. Matter* **14**, 12485 (2002).
- <sup>26</sup>Fortran codes for tridiagonal matrices (after A. Rybicki) are available from <http://www.lanl.gov/DLDSTP/fast/subs.f.txt>. The code for evaluating the determinant may be simply modified to give just its sign.
- <sup>27</sup>G. Martin, A. Botchkarev, A. Agarwal, A. Rockett, H. Morkoç, W. R. L. Lambrecht, and B. Segall, *Appl. Phys. Lett.* **65**, 610 (1994).
- <sup>28</sup>G. Martin, A. Botchkarev, A. Rockett, and H. Morkoç, *Appl. Phys. Lett.* **68**, 2541 (1996).

## Electronic Raman scattering from intersubband transitions in GaN/AlGa<sub>x</sub>N quantum wells

M. P. Halsall<sup>1</sup>, B. Sherliker<sup>1</sup>, P. Harrison<sup>2</sup>, V. D. Jovanović<sup>2</sup>, D. Indjin<sup>2</sup>, Z. Ikonić<sup>2</sup>, T. Wang<sup>3</sup>, M. A. Whitehead<sup>3</sup>, and P. J. Parbrook<sup>3</sup>

<sup>1</sup> Department of Physics, UMIST, PO Box 88, Manchester M60 1QD, UK

<sup>2</sup> Department of Electronic & Electrical Engineering, The University of Leeds, Leeds LS2 9JT, UK

<sup>3</sup> EPSRC National Centre for III–V Technologies, Department of Electronic and Electrical Engineering, Mappin Street, Sheffield S1 3JD UK

Received 10 April 2003, accepted 1 August 2003

Published online 20 October 2003

PACS 73.21.Fg, 78.30.Fs

We present a Raman scattering study of two GaN/Al<sub>x</sub>Ga<sub>1-x</sub>N multiple quantum well (MQW) structures with  $x = 0.3$  and  $x = 0.4$  and well widths of 6 nm and 4 nm respectively, they were nominally undoped but are expected to contain a low-density, n-type, carrier population due to the residual donors in the barriers. Polarization dependent Raman scattering was performed at room temperature, strong scattering due to intersubband transitions (ISBT's) in the GaN quantum wells was observed from both the  $e_1$ – $e_2$  and  $e_1$ – $e_3$  transitions for both samples. The first sample has an  $e_1$ – $e_2$  transition at 300 meV and  $e_1$ – $e_3$  at 480 meV whilst the second sample has an  $e_1$ – $e_2$  transition at 360 meV and  $e_1$ – $e_3$  at 580 meV. The full width half maximum of the Raman peaks is lower than that reported in infra-red absorption for similar, heavily doped, MQW structures.

© 2003 WILEY-VCH Verlag GmbH & Co. KGaA, Weinheim

**1 Introduction** Electronic devices that utilize intersubband transitions (ISBT's) are of increasing technological importance for applications in the Far and Mid infrared regions of the spectrum. The emission/absorption wavelength of an ISBT is only limited by the size of the conduction band offsets of the material system used. Moreover, The devices are unipolar and therefore only the control of n-type doping is required. Since the first demonstration of an intersubband laser (ISBL) in the InGaAs/GaAs system a number of other III–V systems have been used to push the wavelength down to around 3  $\mu\text{m}$  [1–3]. In this respect the AlGa<sub>x</sub>N/GaN system is the center of much current interest as the large offsets in this system allow the production of ISBT's corresponding to wavelengths as short as 1.35  $\mu\text{m}$  [4]. An intersubband laser based on such technology would in, addition to having wide wavelength tunability and high optical power, benefit from the fast carrier dynamics allowing terahertz modulation rates [5]. Although ISBT's have been reported in this region of the spectrum, the production of such devices has not been demonstrated. This is in large part due to the difficulties in operating with a system with such large lattice mismatches and with the thin layers needed to achieve short wavelength ISBT's. For progress to be made in the system prospective device structures need to have their electronic transitions characterized as completely as possible.

The usual technique used to study ISBT's is infrared absorption. Experimentally the technique is relatively straightforward and is generally either done by turning the sample to the Brewster angle and measuring the p-polarised transmission or by waveguiding the light into the sample. The former technique works well in the case of highly doped sample with large numbers of quantum well repeats, so that sig-

\* Corresponding author: e-mail: matthew.halsall@umist.ac.uk

nificant absorption can be measured [6]. The use of waveguiding is more problematic experimentally but is capable of measuring small absorption changes. Indeed, absorption due to  $e_1$ – $e_2$  IS transition in a nominally undoped AlGaIn/GaN high electron mobility structure (single quantum well) were recently reported in this manner [7] as well as absorption due to the  $e_1$ – $e_3$  transition in MQW structure [8].

Here, we report an electronic Raman scattering (ERS) study of two, nominally undoped, GaN/AlGaIn multiple quantum well (MQW) samples designed to have ISBT's corresponding to wavelengths in the vicinity of 3 and 4  $\mu\text{m}$  and with strain balancing condition enforced by employing zero-strain approach [9]. The nominally undoped samples are expected to contain a low background n-type carrier concentration; our own IR absorption measurements were unable to observe the ISBT's due to the low carrier concentrations. The use of the ERS technique, however, allows the observation of both the  $e_1$ – $e_2$  and  $e_1$ – $e_3$  transitions of the structures without any further sample preparation. Moreover, Raman selection rules allow the observation of even parity transitions which are nominally forbidden in absorption measurements. The observed transition energies are modelled using an effective mass model combining the effect of intrinsic electric fields with a self-consistent solution to Poisson's equation for an assumed, low, carrier concentration.

## 2 Experimental procedure

**2.1 Sample growth** All investigated samples were grown on (0001) sapphire substrates by low pressure metalorganic vapour phase epitaxy. Sapphire substrates were initially treated in  $\text{H}_2$  ambient at 1140  $^\circ\text{C}$ , followed by the growth of a 25 nm thick low-temperature (550  $^\circ\text{C}$ ) GaN nucleation layer and a 1.5  $\mu\text{m}$  thick layer of nominally undoped GaN grown at 1050  $^\circ\text{C}$ . Prior to the growth of the AlGaIn/GaN superlattice structure at 1050  $^\circ\text{C}$ , an AlN interlayer of about 20 nm was grown at 600  $^\circ\text{C}$  in order to prevent the crack formation due to the large lattice and thermal expansion coefficient mismatch between AlGaIn and GaN. The MQW structure of the samples grown is detailed in Table 1.

**Table 1** Sample parameters.

sample no.	no. of periods	well width	barrier width
1	10	6 nm GaN	28 nm $\text{Al}_{0.3}\text{Ga}_{0.7}\text{N}$
2	30	4 nm GaN	6 nm $\text{Al}_{0.42}\text{Ga}_{0.58}\text{N}$

**2.2 Raman technique** The Raman spectra were recorded in backscattering geometry from the cleaved sample edge using a Raman microscope system. The 514 nm line of an argon-ion laser was used for excitation. The spectra were analysed for polarization with the growth direction with the polarization axis being parallel to the growth direction ( $x$ ) or at right angles to it ( $y$ ). The spectra were recorded at room temperature.

**3 Results and discussion** Figure 1 shows the Raman spectra obtained from Sample 1, the upper spectrum was recorded under polarized conditions (using standard notation)  $[z(y, y) \bar{z}]$  and the lower spectrum under depolarized  $[z(x, y) \bar{z}]$ . In the figure, there are clearly two features at 300 meV and 480 meV, which are observed under depolarized conditions, as is appropriate for Raman scattering from excitations of single carrier character [10, 11]. Figure 2 shows an equivalent series of spectra for sample 2. The peaks at 500–600 meV (Raman shift) in both spectra are actually emission lines due to Chromium impurities in the sapphire substrate. In the figure the top trace is again recorded in the depolarised geometry, the middle trace is recorded in under polarised conditions, the bottom trace is a subtraction of the polarised from the depolarised scaled so as to remove the chromium emission from the spectrum.

Again in the depolarized spectrum we see a feature, which this time occurs at 360 meV. In the subtracted spectrum there is also a feature at 580 meV, which is obscured the depolarised spectrum by the chromium emission. The observed features from both samples lie close to the expected values for the  $e_1$ – $e_2$  and  $e_1$ – $e_3$  transitions of each sample respectively and we ascribe them to electronic Raman scatter-

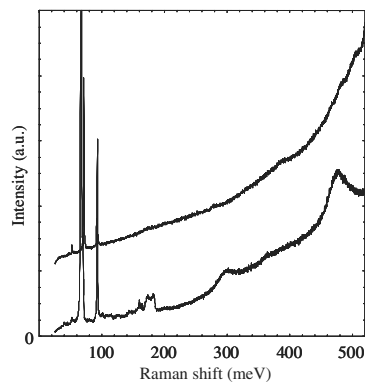


**Fig. 1** Raman spectrum of sample 1 recorded in both polarised (upper trace) and depolarised (lower trace) scattering geometries.

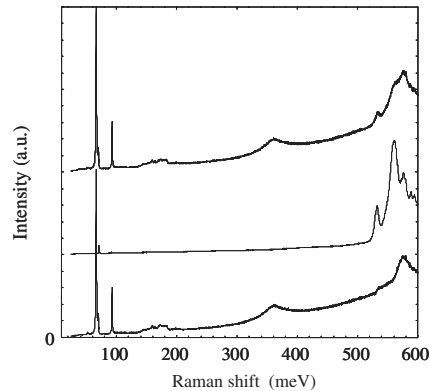


**Fig. 2** Raman spectrum of sample 2 recorded in depolarised (upper trace) and polarised (middle trace) scattering geometries. The lower trace is a scaled subtraction of the polarised spectrum from the depolarised.

ing. The linewidths of these features are remarkably narrow, for example in sample 1  $e_1$ – $e_2$  has a transition energy of 300 meV and a FWHM of 20 meV. In reference 5 ISBT absorption was reported from  $e_1$ – $e_2$  at 306 meV from a nominally undoped AlGaIn/GaN HEMT structure with a FWHM of 86 meV, and in 6 a heavily doped MQW structure was reported to show  $e_1$ – $e_2$  absorption at 300 meV with a FWHM of 96 meV. It can be seen in the figures that scattering intensity due to the  $e_1$ – $e_3$  transition is substantially stronger than that due to the  $e_1$ – $e_2$  transition. The same effect has been observed in the modulation doped AlAs/GaAs system [11] and is a result of the Raman matrix element for scattering via spin density excitations being non-zero only for even parity excitations in the dipole approximation. The odd parity  $e_1$ – $e_2$  transition is only allowed via high order quadrupole terms. This is not necessarily true in the presence of strong resonant Raman effects, in this current system it is unclear which electronic states could be resonant with 2.42 eV excitation and we assume that the scattering is non-resonant.

The observation of electronic Raman scattering has been used in other systems to obtain accurate values of the band offsets in the absence of uncertainties due to exciton binding energies etc. The observed transition energies have been modelled self-consistently by iterative solution of the Schrödinger and Poisson equations with effects of conduction band nonparabolicity included via Kane two band model of an energy dependent effective mass [12, 13]. The large built-in electric fields (~MV/cm) induced by nonlinear piezoelectric and spontaneous polarization was taken into account and calculated from the simple expression assuming periodic boundary conditions over the whole structure [14]. All ternary alloy constants were estimated by employing Vegard's linear law. We assume a conduction band offset  $U_b$  and that Al content in the barrier layer is given as  $x \approx U_b/\Delta E_c$ , where  $\Delta E_c$  is the AlN/GaN conduction band offset, set to be ~2 eV. In calculating the alloy band gap we have included the effect of bowing ( $b = 1$  eV) [15].

By using the described self-consistent model we calculated transition energies based on the specified sample structural parameters varied within the growth uncertainty. The calculated values of  $e_2$ – $e_1$  and  $e_3$ – $e_1$  transition energy are 308 meV and 390 meV for sample 1 and 390 meV and 490 meV for sample 2. It can be concluded that estimated values for  $e_2$ – $e_1$  are in very good agreement with measured transition energies of an average 5% while there is a certain discrepancy (>10%) observed for  $e_3$ – $e_1$  transitions. This is probably due to calculated intrinsic field value uncertainty in the barrier layer which for lower Al content significantly influence the energy position of the second excited state. From the measured data by fitting to values for  $e_2$ – $e_1$  transition energies, conduction band offset can be estimated to be of around 1.95 eV for sample 2 and around 1.8 eV for sample 1.

In conclusion, we have demonstrated the application of Raman scattering to the study of nitride semiconductor intersubband transitions. Two, nominally undoped, structures were studied and, despite the

low residual doping level, scattering due to transitions from the ground state to the first two excited state electron subbands was readily observed from both samples.

**Acknowledgement** The authors would like to acknowledge the support of the Engineering and Physical Sciences Research Council of the UK (contract No. GR/N05215/01).

## References

- [1] J. Faist, F. Capasso, D. L. Sivco, A. L. Hutchinson, S.-N. G. Chu, and A. Y. Cho, *Appl. Phys. Lett.* **72**, 680 (1998).
- [2] F.-Q. Liu, Y.-Z. Zhang, Q.-S. Zhang, D. Ding †, B. Xu †, Z. G. Wang †, D.-S. Jiang, and B.-Q. Sun, *Semicond. Sci. Technol.* **15**, L44 (2000).
- [3] D. Hofstetter, M. Beck, T. Aellen, and J. Faist, *Appl. Phys. Lett.* **78**, 396 (2001).
- [4] C. Gmachl, H. M. Ng, S.-N. G. Chu, and A. Y. Cho, *Appl. Phys. Lett.* **79**, 1590 (2001).
- [5] J. D. Heber, C. Gmachl, H. M. Ng, and A. Y. Cho, *Appl. Phys. Lett.* **81**, 1237 (2002).
- [6] N. Iizuka, K. Kaneko, N. Suzuki, T. Asano, S. Noda, and O. Wada, *Appl. Phys. Lett.* **77**, 648 (2000).
- [7] D. Hofstetter, L. Diehl, J. Faist, W. J. Schaff, J. Hwang, L. F. Eastman, and C. Zellweger, *Appl. Phys. Lett.* **80**, 2991 (2002).
- [8] K. Hoshino, T. Someya, K. Hirakawa, and Y. Arakawa, *phys. stat. sol. (a)* **192**, 27 (2002).
- [9] V. D. Jovanović, Z. Ikonić, D. Indjin, P. Harrison, V. Milanović, and R. A. Soref, *J. Appl. Phys.* **93**, 3194 (2003).
- [10] A. Pinczuk, H. L. Stormer, R. Dingle, J. Worlock, W. Wiegmann, and A. C. Gossard, *Solid State Commun.* **32**, 1001 (1979).
- [11] G. Abstreiter, M. Cardona, and A. Pinczuk, *Light Scattering in Solids IV*, edited by M. Cardona and G. Guntherodt (Springer, Berlin, 1984).
- [12] V. Jovanović, D. Indjin, Z. Ikonić, V. Milanović, and J. Radovanović, *Solid State Commun.* **121**, 619 (2002).
- [13] V. D. Jovanović, Z. Ikonić, D. Indjin, P. Harrison, and R. A. Soref, submitted to *Appl. Phys. Lett.*
- [14] F. Bernardini and V. Fiorentini, *Appl. Surf. Sci.* **166**, 23 (2000).
- [15] F. Yun, M. A. Reshchikov, L. He, T. King, and H. Morkoc, *J. Appl. Phys.* **92**, 4837 (2002).

# **Simulation and design of GaN-based near-infrared quantum well infrared photodetector (QWIP)**

V. D. Jovanović, Z. Ikonić, D. Indjin, P. Harrison

*School of Electronic and Electrical Engineering,  
University of Leeds, Leeds LS2 9JT, United Kingdom*

R. A. Soref

*Sensor Directorate, AFRL/SNHC, Air Force Research Laboratory,  
Hanscom Air Force Base, Massachusetts 01731, U.S.A.*

## **Abstract**

A model for electron transport in quantum well infrared photodetectors with more than one discrete state is presented, based on a scattering rate equation analysis. The important macroscopic parameters like current density, responsivity and capture probability can be estimated directly from a first principles calculation. The applicability of the model was tested by comparison with experimental measurements from a GaN/AlGaN device, and good agreement was found. The model in general can be applied to any other material system or QWIP design.

---

\* Electronic mail: [eenyj@leeds.ac.uk](mailto:eenyj@leeds.ac.uk)

## INTRODUCTION

The recent observations of near-infrared intersubband transitions in wide-band gap group-III nitride semiconductor quantum wells (QWs) [1–6], as well as the experimental verification of theoretically predicted femtosecond carrier dynamics [7–9], confirm that GaN-based materials offer a route for the design of complex optoelectronic devices like ultrafast waveguide switches, optical modulators and even quantum cascade lasers. Moreover, rapid improvements in the growth technology, primarily by using Molecular Beam Epitaxy, make possible the growth of multi-layer structures with considerable quality of the epitaxial layers, delivering controllable widths of the order of a monolayer [10, 11]. This enables investigation of even more complicated intersubband devices [12], like quantum well infrared photodetectors (QWIPs), which would both extend the present range of materials for QWIPs and also the detection wavelengths towards the optical communications range around  $1.55 \mu\text{m}$ . Previous experience in the design of novel quantum devices [13] clearly shows that systematic theoretical modelling is a necessary step towards, improvements of the existing structures [14], and the understanding of physical processes within [15, 16].

In this paper, two main topics are addressed: (i) development of a model for the simulation of electron transport in biased GaN/AlGaIn multi-QW (MQW) systems, giving first principal macroscopic parameters like light and dark current density, responsivity, etc., (ii) design, modelling and experimental verification of a GaN/AlGaIn QWIP for detection in the near-infrared spectral range.

## THEORETICAL CONSIDERATIONS

We consider  $P$  periods of a MQW structure with an externally applied electric field. The energy spectrum of such a system in principal is continuous which makes the exact description of electron behavior virtually impossible. In order to overcome this here we introduce two main approximations: i) that the continuum can be accurately represented with a number of discrete states selected from the continuum by an appropriate boundary condition, ii) that the MQW structure is ideally periodic (and all periods are equivalent), which gives an unique set of states associated to a certain period.

In such a case the electron transport can be simulated by implementing a rate equation approach, from which the electron distribution over quantized continuum states can be in steady-state calculated by solving a system of linear equations as:

$$\frac{dn_i}{dt} = 0 = \sum_{j=1, j \neq i}^N n_j W_{j,i} - n_i \sum_{j=1, j \neq i}^N W_{i,j} + \sum_{k=1}^{P/2-1} \sum_{j=1, j \neq i}^N \{n_j [W_{j,i+kN} + W_{j+kN,i}] - n_i [W_{i+kN,j} + W_{i,j+kN}]\} + \xi \times C(n_1, n_2, \dots) \quad (1)$$

where  $i + kN$  is the  $i$ th state of  $k$ th neighbor period,  $W_{i,j}$  is the total scattering rate from state  $i$  into state  $j$ ,  $n_i$  is the electron concentration of the  $i$ th state and  $\xi$  is equal to 1 for light and 0 for dark conditions. The parameter  $C(\cdot)$  is equivalent to an external perturbation, in our case the concentration of electrons generated per second by the applied optical field. For known electron distributions over continuum states one can estimate macroscopic parameters of the system like current density, capture probability, responsivity etc.

The current density can be calculated by subtracting the current density component due to electrons scattering into the next period from the component due to electrons scattering back, as usually used in quantum cascade laser simulations [16]. As we are dealing with continuum states this approach can be intrinsically unstable. Hence we introduce a different method assuming that average speed of the electron scattering from the state  $i$  to  $j$  is given as

$$\langle v_{ij} \rangle = \frac{\langle z_j \rangle - \langle z_i \rangle}{\tau_{ij}} \quad (2)$$

where  $\tau_{ij}$  is the electron scattering time between states  $i$  and  $j$  ( $\tau_{ij} = W_{i,j}^{-1}$ ),  $\bar{z}$  is an average coordinate of the electron given as

$$\langle z_i \rangle = \int_{-\infty}^{\infty} \psi_i(z) z \psi_i^*(z) dz \quad (3)$$

where  $\psi_i$  is the wavefunction of the  $i$ th state and  $z$  coordinate along the growth direction. Then the current density can be calculated as

$$J = \sum_{k=1}^{P/2-1} \sum_{i=1}^N \sum_{j=1}^N \frac{eN_s}{L} \times \langle v_{ij} \rangle = \sum_{k=1}^{P/2-1} \sum_{i=1}^N \sum_{j=1}^N \frac{eN_s}{L} \times \frac{\langle z_j \rangle - \langle z_i \rangle}{\tau_{ij}} \quad (4)$$

where  $N_s$  is total sheet electron density in one period,  $L$  is the length of the period. This expression defines both the dark and the light current dependent on the value of the parameter  $\xi$ . When the current density is known, the peak responsivity can be expressed as

$$R = \frac{J(\xi = 1) - J(\xi = 0)}{hc/\lambda} \quad (5)$$

where  $\lambda$  is the detection wavelength.

A very important issue is the choice of wavefunctions assigned to a certain period, as the continuum states are not confined within a defined area and the wrong choice can lead to the existence of duplicated states and a false estimation of the carrier dynamics. In order to overcome this potential problem we define states belonging to the considered period as those having the better overlap integral with the ground state of that period than with the ground states of the neighboring periods. For this purpose we define the overlap integral as:

$$O_{ij} = \int_{-\infty}^{\infty} |\psi_i(z)|^2 |\psi_j(z)|^2 dz \quad (6)$$

In order to reduce the number of scattering rate processes necessary to calculate the electron distribution and corresponding current density (note that the number of total scattering rate processes is equal to  $N^2(2P + 1) - N$ ), we introduce the ‘tight-binding’ approximation assuming that only a few closest neighbors interact, and set  $P = 2$ . Also we assumed that electron -longitudinal optical (LO) phonon scattering is the main and only scattering mechanism. Electron-electron scattering was considered to be negligible as the continuum states are hardly populated. The  $k$ -space scattering rate averaging assumed Fermi-Dirac distribution within each subband with a unique electron temperature.

The energies and wavefunctions were calculated by solving the envelope function Schrödinger equation, within the effective mass approximation, with the effects of bulk nonparabolicity via the energy dependent effective mass (two band Kane model) and many-body exchange potential included. The large intrinsic electric field ( $F \sim \text{MV/cm}$ ) induced by the nonlinear piezoelectric and spontaneous polarizations is introduced by assuming periodic boundary conditions over the whole structure [17, 18] as:

$$F_j = \frac{\sum_k (P_k - P_j) l_k / \epsilon_k}{\epsilon_j \sum_k l_k / \epsilon_k} \quad (7)$$

where  $P_i = P_{sp}^i + P_{pz}^i$  is the total polarization given as a sum of piezoelectric and spontaneous (pyroelectric) polarization within a layer of width  $l_i$ . In calculating the alloy band gap we have included the effect of bowing[19].

The optical perturbation constant, in the steady state conditions, is modelled assuming linear dependence on the optical field flux as:

$$C(\Phi, n_i, n_f) = A_{if} \Phi \quad (8)$$

where  $A_{if}$  is fractional optical absorption on the  $i \rightarrow f$  transition which reads:

$$A_{if}(\omega) = \frac{e^2 \omega}{2\bar{n}\epsilon_0 c} |M_{if}|^2 \int_0^\infty L(\hbar\omega, \hbar\omega k_t^2) F_{if}(k_t^2) dk_t^2 \quad (9)$$

where  $\omega_0$  is the transition frequency,  $\hbar$  is the photon energy,  $c$  the velocity of light in vacuum,  $\bar{n}$  the average refraction index,  $M_{if}$  the dipole matrix element,  $k_t$  the transversal (in-plane) wavevector  $\{k_x, k_y\}$ ,  $F_{if}$  is the difference of Fermi-Dirac factors for the two states, and  $L(\cdot)$  the normalized Lorentzian:

$$L(\hbar\omega, \hbar\omega + \hbar k_t^2) = \frac{\Gamma/2\pi}{(\hbar\omega - \hbar\omega_0)^2 + (\Gamma/2)^2}, \quad (10)$$

where  $\Gamma$  is the homogeneous part of the transition linewidth (FWHM), and the transition energy  $\hbar\omega_0$  depends on  $k_t$ , i.e.

$$\hbar\omega_0 = E_{0f} - E_{0i} + \frac{k_t^2 \hbar^2}{2m_{if}}, \quad (11)$$

where  $E_{0f,i}$  denote the state energies at  $k_t = 0$ , and

$$m_{if}^{-1} = m_{||f}^{-1} - m_{||i}^{-1}, \quad (12)$$

is the difference of the reciprocal in-plane (transversal) electron effective masses  $m_{||}$  in states  $i$  and  $f$ . These masses are unequal due to both the nonparabolicity and the position (material) dependence of the band edge effective mass.

The model presented above is based on a first principal calculation with only the optical perturbation as an input parameter. Commonly used methods can not deal with only a few discrete states in the quantum wells [13], which is overcome here by the generality of this approach. It is worth mentioning that a few other authors applied quantum mechanical scattering rate analysis for dark current and capture probability calculations [20, 21], giving no insight into electron transport properties.

## NUMERICAL RESULTS

In this section we present design, theoretical modelling and experimental confirmation of the GaN/AlGaN QWIP. The structure was designed for intersubband transitions between the lowest two subbands of around 250meV corresponding to a wavelength of  $4\mu\text{m}$  in the non-biased conditions. Also the strain-balancing requirement was enforced by using the 'zero-strain' approach [12]. The MQW structure grown by MOVPE [22], consisted of 10 QWs with  $60\text{\AA}$  wide wells and  $280\text{\AA}$  wide barriers. The Al content in the barrier layers was set to 40% giving the equivalent barrier height of 0.75eV ( $\Delta E_c \approx 1.8\text{eV}$ ). The Raman spectroscopy study revealed intersubband transitions at around  $4.1\mu\text{m}$  [22], and confirmed our choice of alloy parameters as well as the application of our self-consistent model for the calculation of intersubband energies and corresponding wavefunctions.

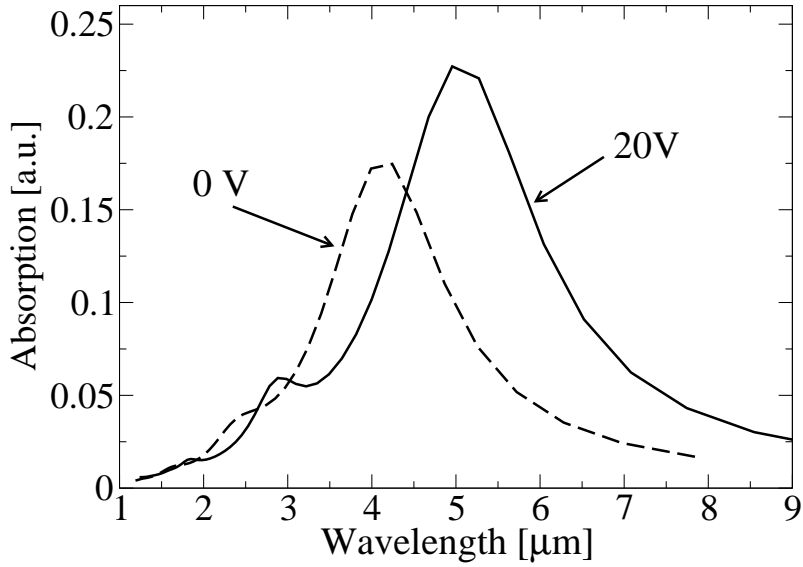


FIG. 1: Calculated absorption profiles for biased (solid line) and non-biased (dashed line) structure.

When an external electric field is applied, a shift of the intersubband transition energies occurs dependent on the strength and polarization of the field. Fig. 1 presents the calculated intersubband absorption profiles (based on the model presented in the previous section) for zero bias and an applied reverse bias of 20V. The estimated blue shift is around  $1\mu\text{m}$  suggesting a wide tunability.

Fig. 2 shows the sample dark current measured at 77K. The I-V curve is asymmetric due to

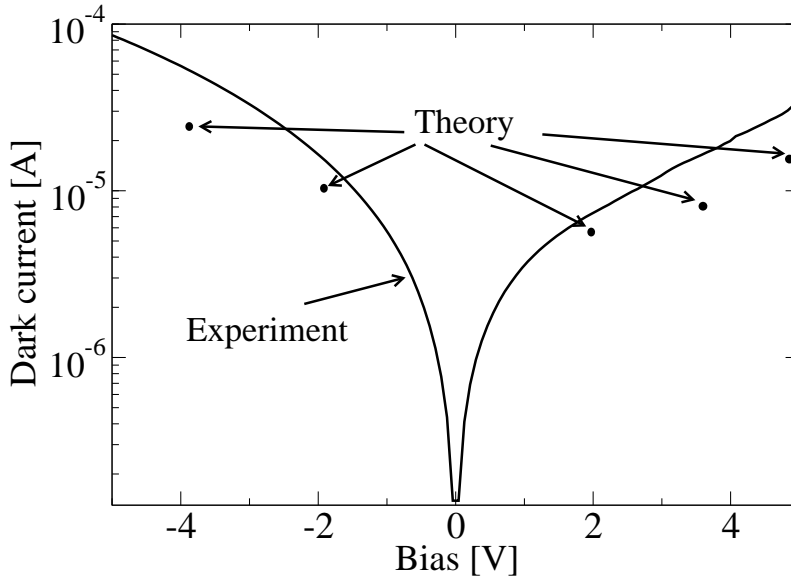


FIG. 2: Measured dark current vs. applied bias at 77K for GaN/AlGaIn QWIP. Dots present theoretical predictions.

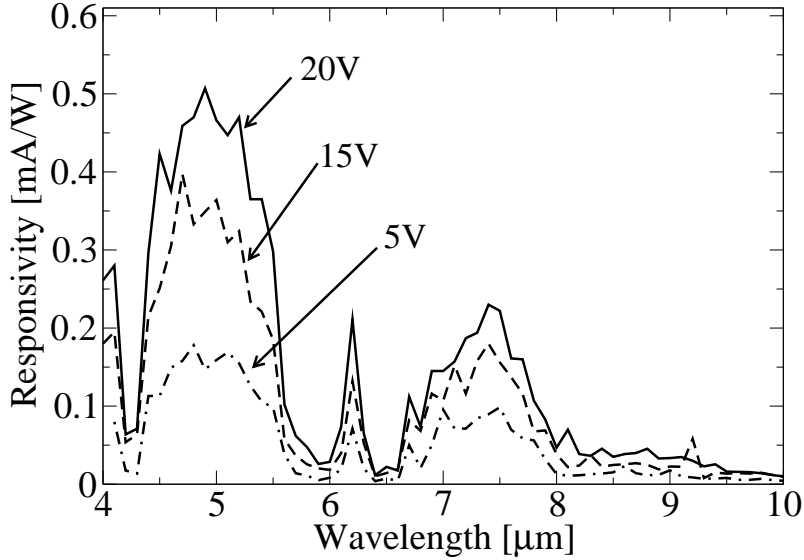


FIG. 3: Measured responsivity vs wavelength for 5 (dot-dashed line), 15 (dashed line) and 20V (solid line) biases.

the intrinsic electric field in the layers, as the electrons can easier switch from the quantum well into continuum, when the externally applied electric fields is of the same polarity as the internal electric field in the barrier. In the working regime above 2V (reverse bias) the value of the dark current is around  $10^{-1}$ mA. The graph also presents theoretical predictions for different values of applied bias and good agreement is found. The slight discrepancy is probably due to other leakage mechanisms (contacts, surface leakage etc.) and are out of the scope of this work. We also estimated the capture probability to be around 30% at 4V and 99% at 1V as expected. The optical response of the sample was examined using the high power source FELIX tunable for wavelengths higher than  $4\mu\text{m}$ . In Fig. 3 are presented responsivity measurements as a function of the source wavelength for different values of the applied bias (note that the dips at  $4.2$ ,  $6$  and  $6.5\mu\text{m}$  are due to atmospheric absorption). It can be seen that for 20V, peak responsivity occurs at around  $5\mu\text{m}$ . With the decrease of applied bias the peak absorption shifts towards shorter wavelengths and as a result the optical response in the range  $> 4\mu\text{m}$  decreases. Fig. 4 shows the calculated responsivity as a function of wavelength for experimentally applied bias values using the microscopical model described in previous section. The optical flux was assumed to be  $\Phi = 10^{18}\text{cm}^{-1}\text{s}^{-1}$  corresponding to the average FELIX pulse power. Again an excellent agreement with the experiment is found for both responsivity profile and absolute values. The continuum states are very weakly populated (lower than 0.01% of the total sheet carrier density within the period) even under high power excitation which opens the question of an unexpectedly high responsivity, especially with energy

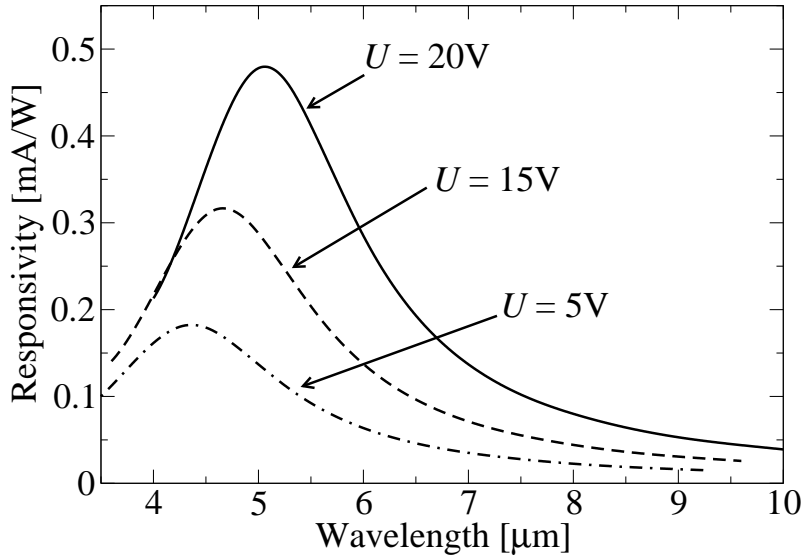


FIG. 4: Calculated responsivity vs. wavelength for different values of applied bias.

spacings between ground and continuum states above 250 meV. By looking into scattering rates as well as current density components we suggest that the high current is due to ultra-fast scattering processes between pairs of continuum states separated by an LO phonon energy.

## CONCLUSION

In conclusion we have presented a first principals fully microscopic model for electron transport in QWIPs with an emphasis on structures with more than one discrete state. The model is based on scattering rate equations with the ‘tight-binding’ approximation applied by including the influence of two nearest neighbors. Macroscopic parameters like current density, responsivity and capture probability are obtained without the need of empirical parameters. In order to examine the accuracy of the simulation we have applied it to a GaN/AlGaIn QWIP, and found excellent agreement with the experiment for dark current and responsivity. The model can generally be applied to any QWIP device.

## ACKNOWLEDGMENT

The authors would like to thank the EOARD and AFOSR for funding. V.D.J. is supported by an ORS award.

- 
- [1] C. Gmachl, H. M. Ng, S.-N. G. Chu, A. Y. Cho, Appl. Phys. Lett. **77**, 3722 (2000).
- [2] C. Gmachl, H. M. Ng, A. Y. Cho, Appl. Phys. Lett. **77**, 334 (2000).
- [3] C. Gmachl, H. M. Ng, A. Y. Cho, Appl. Phys. Lett. **79**, 1590 (2001).
- [4] N. Iizuka, K. Kaneko, N. Suzuki, Appl. Phys. Lett. **81**, 1803 (2002).
- [5] K. Kishino, A. Kikuchi, H. Kanazawa, T. Tachibana, Appl. Phys. Lett. **81**, 1234 (2002).
- [6] K. Kishino, A. Kikuchi, H. Kanazawa, T. Tachibana, Phys. Stat. Sol. (a) **192**, 124 (2002).
- [7] N. Iizuka, K. Kaneko, N. Suzuki, T. Asano, S. Noda, O. Wada, Appl. Phys. Lett. **77**, 648 (2000).
- [8] J. D. Heber, C. Gmachl, H. M. Ng, A. Y. Cho, Appl. Phys. Lett. **81**, 1237 (2002).
- [9] H. M. Ng, C. Gmachl, S. V. Frolov, S. N. G. Chu, A. Y. Cho, IEE Proc.-Optoelectron. **148**, 215 (2001).
- [10] A. Y. Cho, D. L. Sivco, H. M. Ng, C. Gmachl, A. Tredicucci, A. L. Hutchinson, S. N. G. Chu, F. Capasso, J. Crystal Growth **227-228**, 1 (2001).
- [11] H. M. Ng, C. Gmachl, S. N. G. Chu, A. Y. Cho, J. Crystal Growth **220**, 432 (2000).
- [12] V. D. Jovanović, Z. Ikonić, D. Indjin, P. Harrison, V. Milanović, R. A. Soref, J. Appl. Phys. **93**, 3194 (2003).
- [13] L. Thibaudeau, P. Bois, J. Y. Duboz, J. Appl. Phys. **79**, 446 (1996).
- [14] D. Indjin, S. Tomić, Z. Ikonić, P. Harrison, R. W. Kelsall, V. Milanović, S. Koćinac, Appl. Phys. Lett. **81**, 2163 (2002).
- [15] P. Harrison, R. A. Soref, IEEE J. Quantum Electron. **37**, 153 (2001).
- [16] D. Indjin, P. Harrison, R. W. Kelsall, Z. Ikonić, Appl. Phys. Lett. **82**, 1347 (2003).
- [17] V. Fiorentini, F. Bernardini, O. Ambacher, Appl. Phys. Lett. **80**, 1204 (2002).
- [18] F. Bernardini, V. Fiorentini, Appl. Surf. Sci. **166**, 23 (2000).
- [19] F. Yun, M. A. Reshchikov, L. He, T. King, H. Morkoc, J. Appl. Phys. **92**, 4837 (2002).
- [20] N. E. I. Etteh, P. Harrison, J. Appl. Phys **92**, 248 (2002).
- [21] M. A. Gadir, P. Harrison, R. A. Soref, Appl. Phys. Lett. **81**, 4272 (2002).
- [22] M. P. Halsall, et al., Phys. Stat. Solidi (c), **1-4** DOI 10.1002 (2003).